CHEMISTRY
A EUROPEAN JOURNAL

DOI: 10.1002/chem.200903522

The Wacker Process: Inner- or Outer-Sphere Nucleophilic Addition? New Insights from Ab Initio Molecular Dynamics

Aleix Comas-Vives,[a] András Stirling,*[b] Agustí Lledós,[a] and Gregori Ujaque*[a]

Abstract: The Wacker process consists of the oxidation of ethylene catalyzed by a Pd^{II} complex. The reaction mechanism has been largely debated in the literature; two modes for the nucleophilic addition of water to a Pd-coordinated alkene have been proposed: *syn*-inner- and *anti*-outer-sphere mechanisms. These reaction steps have been theoretically evaluated by means of ab initio molecular dynamics combined with metadynamics by placing the $[Pd(C_2H_4)Cl_2(H_2O)]$ complex in a box of water molecules, thereby resembling experimental conditions at low $[Cl^-]$. The nucleophilic addition has also been evaluated for the $[Pd(C_2H_4)Cl_3]^-$ complex, thus revealing that the water by chloride ligand substitution *trans* to ethene is kinetically favored over the generally assumed *cis* species in water. Hence, the resulting *trans* species can only directly undertake the outer-sphere nucleophilic addition, whereas the inner-sphere mechanism is hindered since the attacking water is located *trans* to ethene. In addition, all the simulations from the $[Pd(C_2H_4)Cl_2(H_2O)]$ species (either *cis* or *trans*) support an outer-sphere mechanism with a free-energy barrier compatible with that obtained experimentally, whereas that for the inner-sphere mechanism is significantly higher. Moreover, additional processes for a global understanding of the Wacker process in solution have also been identified, such as ligand substitutions, proton transfers that involve the aquo ligand, and the importance of the *trans* effect of the ethylene in the nucleophilic addition attack.

Keywords: ab initio calculations · hydroxypalladation · molecular dynamics · nucleophilic addition · Wacker process

Introduction

The Wacker process is paradigmatic because it is the first organometallic catalytic oxidation to have been industrially applied.[1] This process involves the oxidation of ethylene to acetaldehyde in aqueous solvent. Its catalytic cycle as currently understood is shown in Scheme 1. Over more than forty years, its mechanism has been the subject of intense debate and very recently its controversial nature has been called into question again.[2] The reaction law has been shown to depend on the reaction conditions, in particular on the concentration of $[Cl^-]$ and $[CuCl_2]$.[3–5] The most controversial reaction step is the hydroxypalladation of ethene. The debate relies on the mode of the water nucleophilic attack on ethene: 1) by means of an inner-sphere mechanism from a coordinated water to palladium (*syn* addition), or 2) by means of an outer-sphere mechanism of a water molecule from the bulk (*anti* addition).[6,7] The determination of the reactivity of the free and coordinated water toward the alkene is crucial in understanding the mechanism and may help to develop other aqueous-phase processes, a key challenge in green chemistry.

The rate law for the process under industrial conditions (low concentration of Cl^- and $CuCl_2$) is that shown in Equation (1). The groups of Stille and Bäckvall independently reported stereochemical studies that supported the outer-sphere attack. The reaction conditions in the case of Stille's group were under high CO pressure that could somehow hinder the nucleophilic inner-sphere attack by coordination of CO molecules to the metal complex; Bäckvall's group performed the experiments at high Cl^- and $CuCl_2$ concentrations.[8–10] In their studies, Bäckvall and co-workers sug-

[a] Dr. A. Comas-Vives, Prof. Dr. A. Lledós, Dr. G. Ujaque
Unitat de Química Física, Departament de Química
Universitat Autònoma de Barcelona,
08193 Bellaterra, Catalonia (Spain)
Fax: (+34) 935812920
E-mail: gregori@klingon.uab.es

[b] Dr. A. Stirling
Chemical Research Center of HAS
Pusztaszeri út 59–67, 1025 Budapest (Hungary)
Fax: (+36) 13257554
E-mail: stirling@chemres.hu

Supporting information for this article is available on the WWW under http://dx.doi.org/10.1002/chem.200903522.

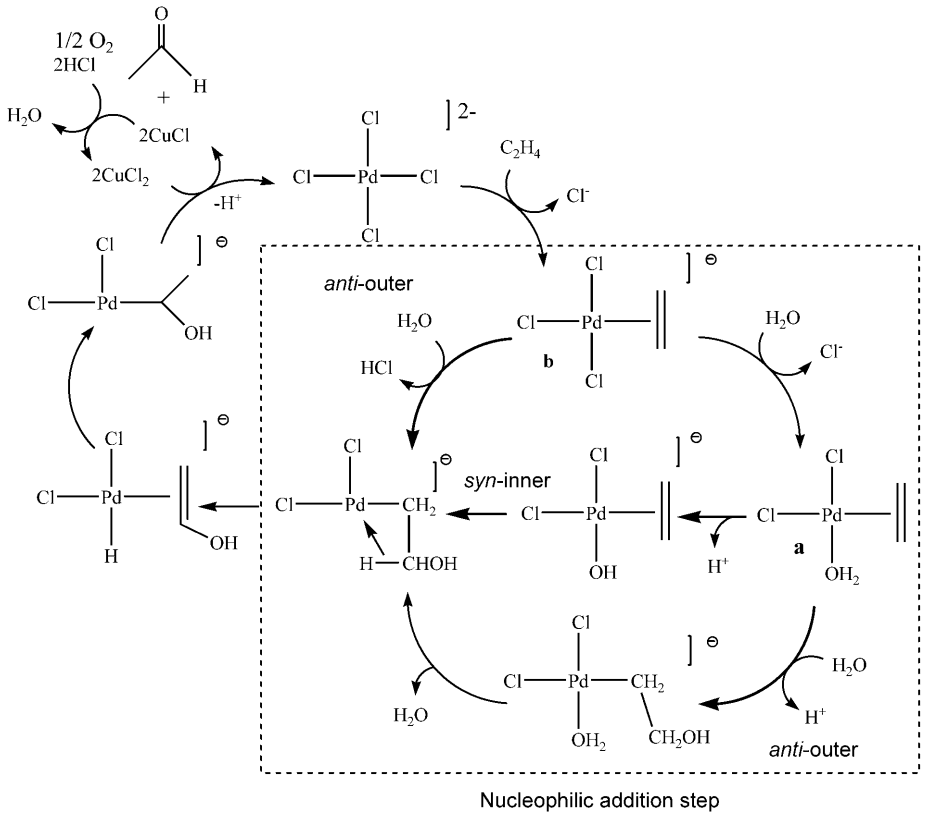

Scheme 1. General catalytic cycle of the Wacker process.

Abstract in Catalan: *El procés de Wacker consisteix en l'oxidació de l'etilè catalitzada per un complex de* Pd^{II}*. El mecanisme d'aquesta reacció ha estat extensament debatut, havent-se proposat dos modes possibles d'addició nucleòfila: en* syn *d'esfera interna i en* anti *d'esfera externa. En aquest treball ambdues etapes de reacció s'han estudiat teòricament mitjançant dinàmica molecular ab initio acoblada a metadinàmica, tot situant el complex* $[Pd(C_2H_4)Cl_2(H_2O)]$ *en una caixa d'aigües emulant les condicions experimentals a baixa concentració d'ió clorur. L'addició nucleòfila també s'ha avaluat en el cas del complex* $[Pd(C_2H_4)Cl_3]^-$*, fet que ha revelat que la substitució d'una aigua del medi pel lligand clorur en* trans *respecte l'etilè es veu afavorida cinèticament respecte l'espècie que generalment s'assumeix com a inicial (l'espècie* cis*). Per tant, a l'obtenir l'espècie* trans*, aquesta tan sols pot donar l'addició nucleòfila d'esfera externa ja que l'addició d'esfera interna necessita l'aigua que s'ha d'addicionar en posició* cis *respecte l'etilè. A més, totes les simulacions partint del complex* $[Pd(C_2H_4)Cl_2(H_2O)]$ *(tan en* cis *com en* trans*) tenen una barrera d'energia lliure compatible amb l'obtinguda experimentalment, mentre que l'associada al mecanisme d'esfera interna és significativament més elevada. Finalment, també s'han identificat processos que contribueixen a la comprensió global del procés de Wacker en solució, com ara substitucions de lligands, transferències protòniques que involucren el lligand aquo i l'importància de l'efecte* trans *de l'etilè en l'addició nucleòfila.*

gested that the rate-determining step (rds), a Cl^- dissociation, takes place after the water nucleophilic addition.[9] Conversely, isotope effects reported by Saito and co-workers supported the inner-sphere mechanism under those conditions.[11]

$$\text{rate} = \frac{k[PdCl_4^{2-}][\text{olefin}]}{[H^+][Cl^-]^2} \qquad (1)$$

Henry's group has largely contributed to the study of the reaction mechanism of the Wacker process.[3–7,12] In his seminal work of 1964, he established the rate law shown in Equation (1).[12] Later, Henry studied the rates of isomerization and oxidation of a simple isotopically substituted olefin capable of showing isotopic scrambling, [D_2]allyl alcohol. Based on the observed lack of scrambling, the *anti* pathway was discarded, although this did not rigorously confirm the *syn* mechanism.[4b,c] On further kinetic studies, Henry also found that at high [Cl^-] concentration (>1.5 M) the nonoxidative isomerization product was obtained, thus raising a new rate-law equation with no proton inhibition term [Eq. (2)].[4a] Thus, there was a change on the rate law depending on [Cl^-] concentrations. Accordingly, based on both kinetic and stereochemical studies, Henry proposed that the reaction proceeds through a *syn*-addition mechanism at low [Cl^-] concentrations, whereas at high [Cl^-] concentrations the reaction goes through an *anti*-addition mechanism.[3]

$$\text{rate} = \frac{k[PdCl_4^{2-}][\text{olefin}]}{[Cl^-]} \qquad (2)$$

Concerning the theoretical calculations carried out to analyze this process, molecular orbital analysis by Eisenstein and Hoffmann showed that η^2 to η^1 ethylene slipping was the driving force toward the external nucleophilic attack.[13] Fujimoto and Yamasaki supported *trans* addition for hydroxide.[14] Siegbahn has also tackled the Wacker process by means of DFT calculations including explicit and implicit solvent models, which also supported an outer-sphere mechanism.[15] Kratgen et al. studied a related Wacker reaction catalyzed by palladium acetate in acetic acid and obtained similar results.[16] Eshtiagh-Hosseini et al. raised comparable results using a similar model for the reaction in water,[17] although some of their conclusions have been questioned later.[18] On the other hand, Nelson et al. supported the *syn*

nucleophilic addition attack by means of modified neglect of differential overlap (MNDO) semiempirical calculations.[19] Recently, Oxgaard, Goddard, and co-workers have also studied this process and nicely rationalized the dependence of the addition mode on reaction conditions on the basis of theoretical calculations.[18,20] The *syn* addition was found to be favorable under certain conditions. Note, however, that a correction was included in the calculations to obtain reasonable energy barriers for those steps in which a proton is released to the medium (thus forming a hydronium species); this is for both the *anti* and *syn* transition states.[20b] This shows that the poor description of the solvation energy of H_3O^+ within the implicit solvation model requires additional, a posteriori corrections to obtain reliable values for proton-releasing processes.

Although a great deal of chemical and mechanistic insight has been obtained from these computational studies, the inherent limitations of simplified solvent models[21,22] in treating the reactive bulk medium prevent one from formulating a fully convincing picture for the mechanism. In particular, a proper description of the aqueous medium is crucial, since solvent molecules can actively participate in this particular process. The most common simulation strategy is to explicitly include solvent molecules into the model and follow the reactions by traditional quantum chemical methods; this approach has proven to work properly in many cases.[23–32] Nevertheless, it is possible to go one step further by doing molecular dynamics calculations.[33–41] The aim of this work is to study the nucleophilic addition step by means of first-principles molecular dynamics combined with metadynamics. This framework allows one to properly describe the reactivity of the Pd intermediates involved in the Wacker process as well as the bulk water solvent. Both principal alternatives for the nucleophilic addition step (Scheme 1) have been evaluated: the inner- and outer-sphere mechanisms.

Intermediates **a** and **b** (Scheme 1) with an ethylene coordinated to the Pd^{II} catalyst were taken as starting points for analyzing the nucleophilic addition steps. These complexes were placed into a cubic box of 26 water molecules. According to this model for the system, these calculations should resemble the experiments performed at low [Cl^-] concentrations, and the results should agree with the rate law obtained under these conditions. For the particular case of simulations with intermediate **b**, this species may evolve by undergoing a Cl^-–H_2O ligand substitution to yield intermediate **a** as generally suggested, or by undertaking the nucleophilic addition process itself (see Scheme 1). Car–Parrinello molecular dynamics coupled with metadynamics simulations[42,43] were performed to determine the reactive paths and to obtain the corresponding free-energy barriers for these nucleophilic addition steps.[44]

Computational Details

All molecular dynamics (MD) calculations have been performed within the Car–Parrinello framework.[45] We have used periodic models of the solutions in a cubic unit cell with dimensions of $9.86 \times 9.86 \times 9.86$ Å. The HCTH/120 exchange-correlation functional[46] has been used; it was shown to properly work for aqueous solutions.[47] Only the valence electrons have been treated explicitly and the interaction between the ionic core and valence electrons has been included through norm-conserving Troullier–Martins-type pseudopotentials.[48a] For Pd in particular, we have generated a pseudopotential including the semicore 4s and 4p states, and core radii of 1.31, 1.37, and 1.25 Å were used for the pseudization of the s, p, and d channels, respectively. The pseudopotentials have been tested on small molecules and complexes against all-electron calculations.[48b] The electronic orbitals were expanded in a plane–wave basis set up to a kinetic energy cutoff of 70 Ry. The fictitious electronic mass was 1000 a.u. in the simulations, and the replacement of the hydrogen atoms with deuterium allowed a time step of 0.169 fs. The simulation temperature was in all cases 300 K. The initial configurations for the simulations have been obtained from an equilibration procedure: $6\,H_2O$ molecules have been replaced by Pd^{II} complexes **a** and **b** in a previously equilibrated water system of $32\,H_2O$ molecules. It was then kept at 600 K for 1 ps and was subsequently cooled down to 300 K over 1.5 ps using velocity rescaling. The temperature employed in all subsequent simulations was 300 K. For the simulations we have used the CPMD program package.[49] The methodology has been already verified for the both main-group and organometallic reactions including various Pd-containing systems either in gas or condensed phases.[50]

In metadynamics[42] we selected a set of collective variables (CVs) s_α. To describe a chemical reaction, the selected CVs must distinguish between reactants and products. In our study we have coupled the metadynamics with ab initio MD within the Car–Parrinello framework. The complete system of the ionic, electronic, and CV degrees of freedom is described by the following equation [Eq. (3)]:

$$L = L_{CP} + \tfrac{1}{2}\sum_\alpha M_\alpha \dot{s}_\alpha^2 - \tfrac{1}{2}\sum_\alpha k_\alpha (s_\alpha(R) - s_\alpha)^2 - V(t,s) \quad (3)$$

L_{CP} is the Car–Parrinello Lagrangian; the first additional term represents the fictitious kinetic energy of the s_α values, in which M_α is the corresponding fictitious mass parameter. The second additional term represents a restraining potential that forces the ionic degrees of freedom to follow the motion of the CVs. We have used M_α and k_α values equal to 50 amu bohr^{-2} and 5 au, respectively, in all the simulations. These parameters ensure the adiabatic separation of the CV movements from the fictitious electronic degrees of freedom of the CP Lagrangian and the necessary correlated motion of the CVs and the auxiliary variables. $V(t,s)$ is a history-dependent potential term that enhances the sampling of the configurational space, thereby encouraging the system to visit unexplored regions of this space. In practice, it is a sum of repulsive hill-like (Gaussian) potential terms deposited at given time intervals [Eq. (4)]:

$$V(t,s) = \sum_{t_i<t} h \exp\left(-\frac{s(t)-s(t_i)}{2(w(t_i)\,\delta s)^2}\right) \quad (4)$$

in which h is the hill height and δs is the hill width. Concerning the hill size, preliminary calculations were performed with larger hill heights and widths, followed by subsequent refinements. All the calculations have finally employed a maximum hill width (δs) of 0.05 and hill heights (h) of 0.314 kcal mol^{-1} except for the **S1** simulation in which a hill height of 0.628 kcal mol^{-1} was used. The nonspherical nature of the free-energy basins was taken into account by employing anisotropic scaling factors (w), which were recalculated in progress at given periods during the simulations as built into the metadynamics routine of the CPMD package. The hills were deposited after 80 MD time steps (13.6 fs) in all the simulations. We estimated a 2.6 kcal mol^{-1} error bar for the calculated activation free energies when using the smaller Gaussian height.[51] During the metadynamics simulations, we explored the free-energy surface spanned by the selected CVs. As the simulation proceeded we gradually explored this surface by reconstructing it from the deposited Gaussian hills [Eq. (5)]:

$$F(s) = -\lim_{t\to\infty} V(t,s) + \text{const.} \quad (5)$$

This is graphically depicted in Figure 1.

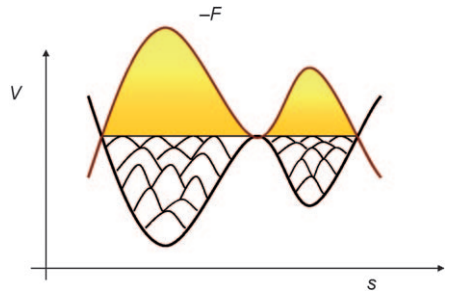

Figure 1. Graphical representation of $V(t,s)$ as the sum of localized Gaussian functions that reconstruct the free-energy surface. In this 1D example, the selected collective variable S allows us to go from one well to another.

For every elementary step we can therefore determine the corresponding activation free energy irrespective of the order of the reaction steps. In this study, the activation free-energy values are reported relative to the free-energy level of the initial species. For the nucleophilic addition steps, we have checked that the predicted transition state structures indeed connect the corresponding minima in dynamical sense; we have performed commitment analysis by selecting representative configurations from the transition-state (TS) regions and then started unbiased MD simulations that employed random atomic velocities taken from the 300 K Boltzmann distribution. These simulations produced trajectories that arrived into the two free-energy minima in almost equal times; this indicates that the selected CVs indeed identified the proper TS between the reactant and product states.

Properly selected CVs can dramatically accelerate reactive events and obtain the corresponding activation free-energy barriers.[43] We have applied different CVs in several combinations to probe the possible mechanisms. For **a**, the selected CVs are the coordination number (CN)[44] of the oxygen of the H_2O ligand with respect to all H atoms (CV1), CN of the ethene carbon atoms with respect to the oxygen of the H_2O ligand (CV2), CN of the Pd atom with respect to the Cl atoms (CV3), CN between the carbon atoms of the ethene and all oxygen atoms (CV4), CN of the Pd atom with respect to all oxygen atoms (CV5), and CN of the Pd atom with respect to the oxygen of the H_2O ligand (CV6). For b, analogous CVs to CV3, CV4, and CV5 were selected: CV3′, CV4′, and CV5′. All CVs with their associated chemical changes are summarized in Table 1.

For each metadynamics simulation a set of 2 or 3 CVs has been employed. In all, 6 different combinations of CVs have been compared to look into the hydroxypalladation step; the resulting **S1**–**S6** combinations are depicted in Scheme 2. Note that in a metadynamics simulation the observable reactions are determined by the selected CV sets, thus different sets generate different sequences of reactions steps.

Table 1. Description of the chemical changes associated to the collective variables (CVs).

	Chemical changes associated with the CVs
CV1	acid–base properties of the aquo ligand
CV2	inner-sphere nucleophilic attack of the aquo ligand to ethene
CV3 and CV3′	Cl^- ligand-substitution processes
CV4 and CV4′	outer-sphere nucleophilic attack of bulk water to ethene
CV5 and CV5′	additional water coordination to Pd
CV6	aquo ligand substitution

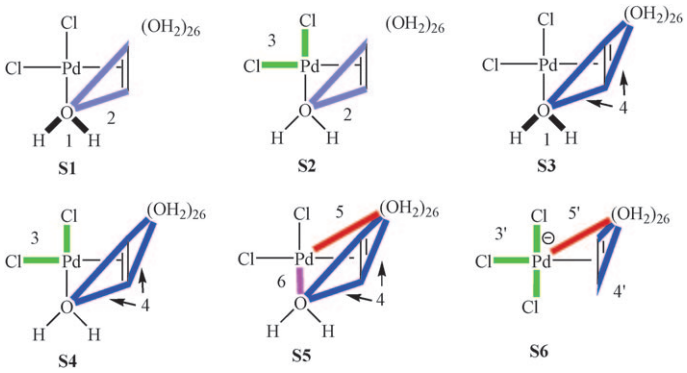

Scheme 2. Selected set of CVs for **a** (simulation **S1** to **S5**) and **b** (simulation **S6**) complexes.

Results and Discussion

We first summarize the results concerning the chemical activity of the Pd^{II} coordination sphere in species **a**, because this is the intermediate generally depicted in the textbook reaction mechanism for the Wacker process. Several ligand-substitution processes were observed during all these simulations. The Cl^-–H_2O ligand exchange *trans* to ethene requires a free-energy barrier of 14 kcal mol^{-1}, whereas that *cis* to ethene requires 35 kcal mol^{-1}, respectively. This indicates that the *trans* substitution process is rather easy in solution, whereas the *cis* one is much more difficult. The 21 kcal mol^{-1} activation energy difference implies approximately 15 orders of magnitude difference in the ligand-exchange rates and indicates that the well-known strong *trans* effect of the ethylene ligand is likely playing a key role in the reaction mechanism.[52,53] Whereas direct experimental data are not available for this complex, data for the analogue Pt^{II} complexes also show this remarkably large *trans* effect of the ethylene ligand.[54] The degenerate H_2O–H_2O exchange features a barrier of 25 kcal mol^{-1}. We have also found that a coordinated water molecule can easily transfer a proton to the solvent: the corresponding free-energy barrier is 10 kcal mol^{-1}. The experimental energy barrier for the deprotonantion of a closely related complex, $[PtCl_3(H_2O)]^-$, is 9.6 kcal mol^{-1}. The agreement between the experimental and theoretical values is remarkable and implies that our methodology properly describes proton-transfer processes in inorganic complexes.[55–62] The protonation of the H_2O ligand should overcome a barrier of 13 kcal mol^{-1}. Taken into account the experimental value of the addition step (22.4 kcal mol^{-1})[11a] and the accuracy of the simulations[44] we conclude that these processes can in fact alter the stoichiometry of the catalyst species before the addition reaction takes place and therefore the actual simulations should include these possibilities.

S1 and **S2** simulations were designed to study the intramolecular mechanism. In the first metadynamics simulation for species **a** (**S1**), we have observed an inner-sphere nucleophilic addition (CV2) preceded by a couple of proton exchanges with the bulk (CV1). The coordinated water was rapidly deprotonated to form a hydroxyl ligand, which then reacted with the ethylene ligand. After that, the *syn*-addition product was obtained with a calculated free energy barrier of 60 kcal mol^{-1}, much higher than the experimental value. Figure 2 shows a representative configuration of the transition-state region. Note that the attack takes place after the facile proton transfer from the aquo ligand to the medium (with a barrier less than 10 kcal mol^{-1}). During these simulations, we observed a *syn* attack of the OH^- ligand to the ethylene. The set of CVs was also compatible with a direct aquo ligand attack to the ethylene accompanied with a proton transfer, but we could not observe this sequence, which indicates an even higher barrier for such a mechanism.

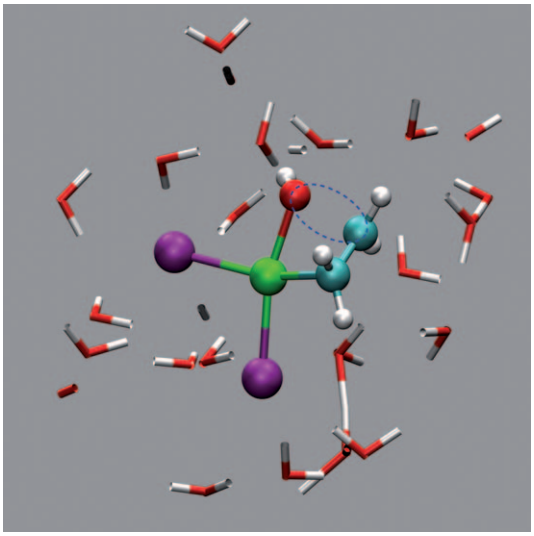

Figure 2. Snapshot of one configuration in which the inner-sphere attack on ethene is occurring (**S1** simulation). The Pd^{II} complex is shown in ball-and-stick representation, whereas the solvent molecules are represented with simple tubes. Green: Pd, red: O, blue: C, magenta: Cl, white: H atoms. The blue ellipse indicates the region in which the C–O bond formation takes place. Fragment solvent molecules are occurring due to the periodic boundary conditions; note that fragment H atoms are not shown for clarity.

The **S2** simulation includes the Cl^- coordination around the Pd^{II} ion (CV3) together with CV2 governing the inner-sphere attack. The simulations revealed large Cl^- mobility and frequent dissociation from the first solvation shell preceding the inner-sphere attack. The free-energy barrier for this latter process was found to be 48 kcal mol^{-1}. This barrier is too high in comparison with the experimental Gibbs energy barrier for the Wacker process (22.4 kcal mol^{-1}).[11a] Due to this high barrier, the formation of triply hydrated, doubly charged Pd^{II} species was observed during the simulation before the intramolecular addition. This species, however, rapidly took up a Cl^- anion and released a proton to the solvent. Such a charge separation featuring 35 kcal mol^{-1} barrier is highly unfavorable and indicates that this sequence is very unlikely. Clearly, both **S1** and **S2** suggest that the inner-sphere mechanism is not compatible with the experimental Gibbs energy barrier.

In the following four simulations, we probed the outer-sphere (intermolecular) mechanism. The **S3** simulation includes CV1 and CV4 steering the proton exchange of the water ligand and the nucleophilic attack on the ethylene ligand, respectively. The difference between **S1** and **S3** is that in the latter case all H_2O molecules (coordinated and free) can attack the ethylene ligand. The simulation shows that the first chemically relevant events are proton shuttling between the aquo ligand and the solution, which is in accordance with their smaller activation barriers. The intermolecular nucleophilic attack takes place when a "neutral" water molecule is coordinated as a ligand. This step has a free-energy barrier of 24 kcal mol^{-1}, a value compatible with that obtained experimentally within the error margin of the calculation.[44] The C–O bond formation was accompanied by a proton transfer to a neighboring H_2O molecule. Figure 3 displays a representative snapshot of the transition state of the outer-sphere attack.

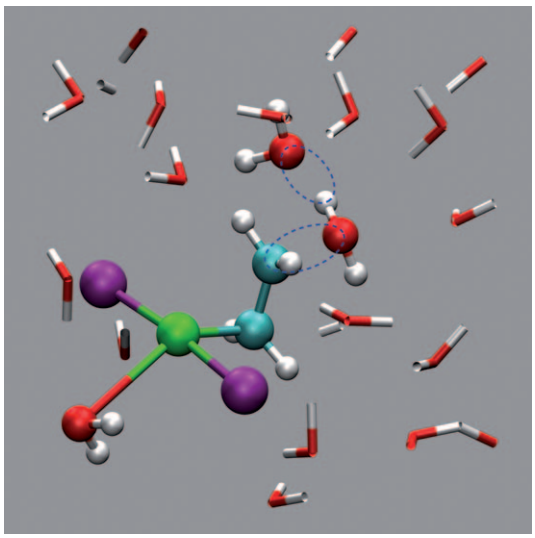

Figure 3. Snapshot of one configuration (**S5** simulation) in which the outer-sphere attack on ethene is occurring. The Pd^{II} complex and the solvent molecules participating in the reaction are shown in ball-and-stick representation, whereas the other solvent molecules are represented with simple tubes. The blue ellipses indicate the regions in which the C–O bond formation takes place and one of the protons of the reactant water jumps to another water molecule. For the coloring scheme and for other visualization details, see Figure 1.

The role of the chloride ligands was also probed in the outer-sphere route. In simulation **S4**, we employed CV3 and CV4. The outer-sphere attack took place with an energy barrier height of 22 kcal mol^{-1}. During the process, we ob-

served a partial decoordination of the Cl^- ligand. We can attribute this to the high *trans* effect of the ethene ligand, which manifests itself under the action of CV3. One of the protons of the attacking H_2O is again spontaneously released into the medium during the addition. The barrier for the outer-sphere attack in this case is very similar to that obtained in **S3** employing a different combination of CVs and is compatible with the experimental value.

In simulation **S5**, we studied the combined effect of three CVs, namely, CV4, CV5, and CV6. The motivation behind this choice was to include not only the reaction coordinates responsible for the intra- and intermolecular attacks, but to also foster possible ligand exchanges on the central Pd^{II} cation (CV5 and CV6). During the simulation, the inner-sphere attack did not occur in line with its high barrier; instead the outer-sphere attack could be observed with an energy barrier of 22 kcal mol^{-1}, which is in very good agreement with previously calculated values. This step gives rise to the *anti* addition product. The simulation yielded a proton release from the attacking H_2O molecule to the solvent during the addition reaction. Moreover, a Cl^-–H_2O exchange in the early stage of the simulation was also observed. The recoordination of the dissociated Cl^- ion took place in the *trans* position with respect to the other chloride ligand, thereby giving rise to the *trans*-$[Pd(C_2H_4)Cl_2(H_2O)]$ intermediate. This recoordination to form the *trans* complex took place before the nucleophilic addition. Note that this simulation suggests that the nucleophilic addition step occurs on a complex with the ligands in *trans* arrangement. These results are fully consistent with the rate law because the calculations show that two Cl^- ligands are released during the process. In addition, we also observed during the simulation an H_2O exchange on the $[Pd(C_2H_4)Cl(H_2O)_2]^+$ intermediate.

The simulation starting from intermediate **b** turned out to be illustrative for a better understanding of the process. From intermediate **b** the unique possible pathway for the nucleophilic attack is the outer-sphere mechanism, provided that no *cis*-Cl^-–H_2O substitution occurs beforehand. A simulation (**S6**) was carried out and involved chloride coordination (CV3′), water coordination (CV5′), and the nucleophilic attack of a water molecule to the coordinated ethene (CV4′). The first step observed during the metadynamics run was the substitution of the *trans*-chloride ligand of intermediate **b** by a water molecule to yield *trans*-$[Pd(C_2H_4)Cl_2(H_2O)]$; this result is in accord with that of simulation **S5**. This configuration excludes an inner-sphere nucleophilic attack, but is suitably disposed for an outer-sphere nucleophilic attack. Subsequently we observed the outer-sphere nucleophilic attack of a solvent H_2O to the coordinated ethene along with the proton transfer to the medium. Interestingly, nucleophilic attack took place on the neutral complex with a free-energy barrier of 19 kcal mol^{-1}. This value is somewhat lower than that obtained for intermediate **a** and it is fully compatible with experiments within the error margin[44] of the simulations.

An important conclusion from this simulation is that the outer-sphere attack takes place on the *trans*-$[Pd(C_2H_4)Cl_2(H_2O)]$ complex and not on the $[Pd(C_2H_4)Cl_3]^-$ or on the *cis*-$[Pd(C_2H_4)Cl_2(H_2O)]$ complexes, although both processes were allowed during the simulation. This result suggests that complex **b** forms first the *trans*-$[Pd(C_2H_4)Cl_2(H_2O)]$ intermediate, and this is the accessible species for nucleophilic attack. Formation of *cis*-$[Pd(C_2H_4)Cl_2(H_2O)]$ certainly cannot be excluded, although it requires a more complicated pathway. The strong *trans* effect of ethylene prevents the direct formation of the *cis*-$[Pd(C_2H_4)Cl_2(H_2O)]$, thereby hindering in this way the inner-sphere nucleophilic attack. Clearly, this step leads the reaction through the outer-sphere nucleophilic addition channel. This result nicely agrees with a very recent theoretical work in analogous Pt^{II} complexes in which ethene has been shown to have the highest *trans* effect and water the lowest one.[63]

To further investigate the origin of the differences between the inner- and outer-sphere mechanism, we analyzed how the electron density is affected on going from the reactant to the transition state. In Figure 4 we show how significant the density changes are around the Pd^{II} ion to reach the transition-state region of the inner mechanism (Figure 4A) as opposed to the small changes that occur during the outer mechanism (Figure 4B). Indeed, in the latter process the Cl^- and H_2O ligand fluctuations yield larger density changes than the ethene reorientation. During the inner mechanism, the ethylene ligand rotates and shifts toward the neighbor ligand OH, thus strongly affecting its hydrogen-bond structure and also repelling nearby water molecules. On the contrary, during the outer mechanism, the solvent shell is maintained and large rearrangements in the solvation structure are not required. Such reorganization can partially account for the free-energy difference between the two mechanisms.

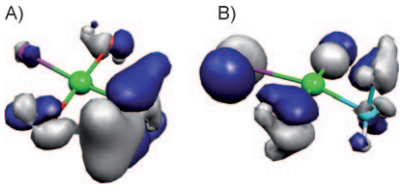

Figure 4. Density difference calculated from the total electronic density of representative configurations of the TS and reactant states: A) inner mechanism (**S2**); B) outer mechanism (**S4**). The density contours are plotted using an 0.04 au cutoff. The gray and blue regions indicate positive and negative values, respectively. For the coloring scheme of the atoms, see Figure 1.

The simulations have revealed that the solvent plays an additional important role in the mechanism. The intermolecular reactions always involved a proton departure from the attacking water to a nearby solvent molecule when the addition to the double bond occurred. This is illustrated in Figure 5, which displays the typical curves of the simultaneous C–O bond formation and proton transfer in simulation

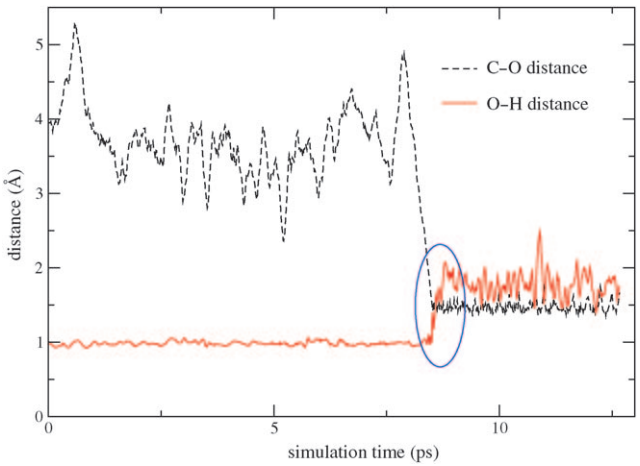

Figure 5. Evolution of the C–O bond and one of the O–H bonds of the reactant H_2O molecule in simulation **S4**. Note that the curves represent configurations taken at every metadynamics step, namely, every 13.6 fs. The blue ellipse indicates the TS region. Similar concerted behavior has been found for all the other intermolecular cases.

S4. This concerted behavior highlights the importance of the second and further neighbor water molecules in the reaction, as the proton transfer is an essential part of the addition reaction and the accompanying charge separation due to the proton-transfer benefits from the presence of the polar water medium. We conclude that explicit inclusion of the surrounding bulk water is critical in the simulations to efficiently contrast the solvent effects for the inner and outer mechanisms and to obtain the concerted nature of the C–O formation step of the outer mechanism in a fairly unbiased manner.

The above results indicate that the inner-sphere mechanism is not feasible for the hydroxypalladation step. Although this step is usually assumed to proceed from species **a**, the simulations indicated that formation of **a** from the $[Pd(C_2H_4)Cl_3]^-$ complex cannot take place in a single step. The actual distribution of the *cis*- and *trans*-$[Pd(C_2H_4)Cl_2(H_2O)]$ is of course determined by the equilibria of the steps that constitute their interconversion.[64] This implies that the presence and reactivity of **a** have to be taken into consideration. However, our calculations also revealed that the inner-sphere mechanism is highly unfavorable for **a**. Simulation on the direct hydroxypalladation step starting from **b** showed again that the only reasonable path is the outer-sphere mechanism due to the structural constraint in the *trans* configuration. Clearly, for both isomers the inner-sphere mechanism can be safely ruled out on the basis of the calculations.

To connect this to experimental data, a critical requirement is that our results must be in accord with the overall rate law [Eq. (1)]. The rate dependence on concentrations $[PdCl_4]^{2-}$, [olefin], and $[Cl^-]$ can be explained by the formation of the $[Pd(C_2H_4)Cl_2(H_2O)]$ complex (either *cis* or *trans*). More difficult to account for is the inverse proton concentration dependence, which points to a deprotonation step. All simulations showed that the hydroxypalladation occurs on the neutral complex; it features a proton transfer at the transition state in concert with the C–O bond formation. The problem as to whether this proton transfer is related in some way to the kinetically observed proton inhibition cannot be decided from the present calculations; the overall reaction mechanism is needed for that. The outer mechanism can be brought into agreement with the rate law for the process if we assume subsequent steps of similar (or slightly higher) activation energy that contribute to the overall rate law. In this scenario, the only requirement is that the activation energies of the steps that lead to hydroxypalladation do not exceed the experimentally observed value (22.4 kcal mol^{-1}). Consider for example, the reaction proceeding from **b** (see Scheme 3): The H_2O–Cl substitution has a free-energy barrier of 14 kcal mol^{-1}, whereas the subsequent nucleophilic addition step requires 19 kcal mol^{-1}. In fact, this is in agreement with experimental results since these free-energy barriers within the error margin[44] are not higher than that reported experimentally. Note that in this scenario the hydroxypalladation step is not the sole rate-determining step, but it is one in a sequence of reaction steps that determines the overall reaction rate. Indeed, Bäckvall proposed the Cl^- ligand release after the nucleophilic addition and prior to the formation of a Pd–hydride intermediate as the rate-determining step at high Cl^- concentrations.[9] Accordingly, subsequent reaction steps need to be studied in detail to have an overall picture of the whole reaction mechanism. In this scenario, the free-energy barriers obtained for the outer-sphere nucleophilic addition mechanism on the *trans* complex are fully consistent with both the rate law and the experimental Gibbs energy barrier of the process. However, further studies are required to assess the validity of this assumption.

We finally note that the selected CVs do not distinguish between the *syn* and *anti* attacks but only between the inner- and outer-sphere routes. Hence, the *syn* outer-sphere

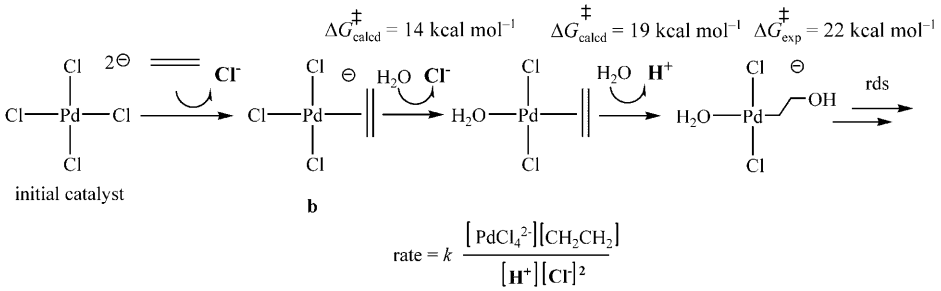

Scheme 3. Proposed sequence of steps with their calculated free-energy barriers for the water nucleophilic addition to coordinated ethene. The rate law at our operating reaction conditions is shown at the bottom part of the scheme. The species with inverse reaction dependence on the reaction rate are shown in bold. The above-depicted reaction scheme fits with the observed rate law.

attack can not be fully discarded as a feasible reaction pathway. We note, however, that the CVs in fact allow both the *syn* and the *anti* directions. Since only the *anti* addition has been observed in the **S3**–**S6** simulations, the *syn* attack has necessarily a higher energy barrier.

The present findings unequivocally support the mechanistic concept that invokes an outer-sphere, *anti*-addition route for the C–O bond formation. Note that our results do not agree with the conclusions reported by Henry on the reaction mechanism on the Wacker process at low Cl^- and $CuCl_2$ concentrations. During the thoughtful work performed by Henry on the reaction mechanisms, two reasonable assumptions were adopted: 1) the coordinated aquo ligand should be in the *cis* position related to ethene, and 2) a Pd–OH species should be a stable intermediate under acidic conditions. The initial formation of the *cis* intermediate, however, is not supported by the present calculations; *trans*-[Pd(C_2H_4)Cl_2(H_2O)] complex is clearly kinetically and thermodynamically the most favored species.[64] Regarding the second assumption, recent experiments performed by Cruywagen and Kriek indicate that at low pH conditions the protonated Pd–H_2O species is the preferred one.[65] Note also that Henry's reagents could also tautomerize providing a incorrect proof.

Another important point for the mechanism concerns the nucleophilic attack and whether or not this is a reversible process. According to the experiments performed by Henry on [D_2]allyl alcohol, the nucleophilic addition cannot be an equilibrium process because deuterium scrambling was not observed. This is taken as proof supporting the *syn* addition for the process. The results from these experiments do not unequivocally mean that the reaction goes through the *syn* pathway. In spite of the fact that this assumption is quite reasonable, the behavior of the allylic alcohol does not necessarily match that of the ethene. Actually, it has been confirmed that the directing influence of hydroxide groups could affect epoxidations, hydrogenations, and oxidation reactions.[66]

Thus, the debate on the reaction mechanism for the Wacker process is still open according to these theoretical calculations and the conclusions obtained by the interpretation of the experimental results. Additional theoretical calculations are needed for the subsequent steps of the reaction mechanism to have a general overview of the overall process with the intent to accommodate both experimental observations and theoretical results.

Conclusion

In conclusion, with DFT-based molecular dynamics simulations, we have followed both the intra- and intermolecular pathways for the nucleophilic attack on the coordinated ethene ligand in the Wacker process. Our main findings are the following:

The ligand sphere of Pd^{II} may undergo several changes before reactions on the ethene ligand occur. It must be stressed that the experimental conditions most resembling our simulations are those at low [Cl^-] and [$CuCl_2$] concentrations.

For both the *cis*- and *trans*-[Pd(C_2H_4)Cl_2(H_2O)] isomers, the outer-sphere mechanism is predicted. For the simulations starting from intermediate **a** (*cis*-[Pd(C_2H_4)Cl_2(H_2O)]) the calculated free-energy barrier for an outer-sphere process ranges between 22 and 24 kcal mol^{-1}, which is in accord with the reported experimental value (22.4 kcal mol^{-1}), whereas the barrier for an inner-sphere (*syn*) nucleophilic attack is clearly higher.

For the *trans* isomer, a feasible outer-sphere nucleophilic addition with a free-energy barrier of 19 kcal mol^{-1} was obtained.

All simulations indicate that the water nucleophilic attack takes place on the neutral complex (simulations assume neutral conditions for the solvent).

We have shown that the formation of the *trans*-[Pd(C_2H_4)Cl_2(H_2O)] isomer is kinetically preferred to the *cis* isomer from intermediate **b**, which is in contrast with the generally depicted *cis*-Cl–H_2O ligand substitution. This fact is indeed remarkable because this intermediate cannot undergo the intramolecular *syn* nucleophilic addition with the coordinated water molecule due to obvious structural reasons. Moreover, another very interesting observation is that the *trans* effect due to ethene is actually hindering the inner-sphere nucleophilic attack, thereby providing very useful insight for the experimental community to develop further active metal catalysts. The possibility of a second Cl–H_2O ligand substitution generating a complex with the ethene and a water ligand in the *cis* position (which has in fact been theoretically observed) cannot be invoked in the reaction mechanism because it would contradict the rate law (it would imply releasing three Cl^- ligands). Generation of intermediate **a** can not be discarded, however; we have also shown that in this case again the outer-sphere attack is also clearly preferred.

The outer-sphere mechanism and the experimentally proposed overall rate law can be brought into agreement by assuming that the overall rate law involves further steps subsequent to the nucleophilic addition. These steps must feature similar activation energies not exceeding the 19–24 kcal mol^{-1} range.

The conclusions reported here are important since they support an *anti* reaction mechanism. We stress that additional theoretical work (in progress) is needed to have an overall picture of the complete reaction so that it can bring into agreement all the experimental observations and theoretical results presented in this study. In light of the present results, we are convinced that the methodology offers a very efficient framework for such studies and will help in broadening our understanding of the Wacker process and other aqueous-phase catalytic reactions.

Acknowledgements

We are grateful to the Spanish MICINN (projects CTQ2008-06866-CO2-01, Consolider Ingenio 2010 CSD2007-00006, FPU fellowship to A.C.-V., and HH2008-0028), to Generalitat de Catalunya (2009/SGR/68), and to the Hungarian Science Foundation (OTKA K 68360). The Red Española de Supercomputación (RES-BSC) is also acknowledged for providing computing time. Fruitful discussion on kinetics with Dr. Gábor Lente and Prof. J. M. Lluch is acknowledged.

[1] a) J. Smidt, W. Hafner, R. Jira, J. Sedlmeier, R. Sieber, R. Ruttinger, H. Kojer, *Angew. Chem.* **1959**, *71*, 176; b) J. Smidt, J. Sedlmeier, W. Hafner, R. Sieber, A. Sabel, R. Jira, *Angew. Chem.* **1962**, *74*, 93; *Angew. Chem. Int. Ed. Engl.* **1962**, *1*, 80; c) R. Jira, *Angew. Chem.* **2009**, *121*, 9196; *Angew. Chem. Int. Ed.* **2009**, *48*, 9034.
[2] J. A. Keith, P. M. Henry, *Angew. Chem.* **2009**, *121*, 9200; *Angew. Chem. Int. Ed.* **2009**, *48*, 9038.
[3] a) O. Hamed, C. Thompson, P. M. Henry, *J. Org. Chem.* **1997**, *62*, 7082; b) O. Hamed, P. M. Henry, C. Thompson, *J. Org. Chem.* **1999**, *64*, 7745; c) O. Hamed, P. M. Henry, *Organometallics* **1997**, *16*, 4903.
[4] a) N. Gregor, K. Zaw, P. M. Henry, *Organometallics* **1984**, *3*, 1251; b) M. Zaw, M. Lautens, P. M. Henry, *Organometallics* **1985**, *4*, 1286; c) W. K. Wan, K. Zaw, P. M. Henry, *Organometallics* **1988**, *7*, 1677; d) J. W. Francis, P. M. Henry, *Organometallics* **1992**, *11*, 2832.
[5] J. W. Francis, P. M. Henry, *J. Mol. Catal. A* **1996**, *112*, 317.
[6] P. M. Henry in *Handbook of Organopalladium Chemistry for Organic Synthesis, Vol. 1* (Ed.: E.-I. Negishi), Wiley, New York, **2002**, pp. 2119–2139.
[7] P. M. Henry in *Palladium-Catalyzed Oxidation of Hydrocarbons: Catalysis by Metal Complexes*, D. Reidel Publishing, Boston, **1980**.
[8] J. K. Stille, D. E. James, *J. Organomet. Chem.* **1976**, *108*, 401.
[9] J. E. Bäckvall, B. Akermark, S. O. Ljunggren, *J. Am. Chem. Soc.* **1979**, *101*, 2411.
[10] J. K. Stille, R. Divakaruni, *J. Organomet. Chem.* **1979**, *169*, 239.
[11] M. Kosaki, M. Isemura, Y. Kitaura, S. Shinoda, Y. Saito, *J. Mol. Catal.* **1977**, *2*, 351.
[12] P. M. Henry, *J. Am. Chem. Soc.* **1964**, *86*, 3246.
[13] O. Eisenstein, R. Hoffmann, *J. Am. Chem. Soc.* **1981**, *103*, 4308.
[14] H. Fujimoto, T. Yamasaki, *J. Am. Chem. Soc.* **1986**, *108*, 578.
[15] a) P. E. M. Siegbahn, *Struct. Chem.* **1995**, *6*, 271; b) P. E. M. Siegbahn, *J. Am. Chem. Soc.* **1995**, *117*, 5409; c) P. E. M. Siegbahn, *J. Phys. Chem.* **1996**, *100*, 14672.
[16] D. D. Kragten, R. A. van Santen, J. J. Lerou, *J. Phys. Chem. A* **1999**, *103*, 80.
[17] a) S. A. Beyramabadi, H. Eshtiagh-Hosseini, M. R. Housaindokht, A. Morsali, *Organometallics* **2008**, *27*, 72; b) S. A. Beyramabadi, H. Eshtiagh-Hosseini, M. R. Housaindokht, A. Morsali, *THEOCHEM* **2009**, *903*, 108.
[18] J. A. Keith, R. J. Nielsen, J. Oxgaard, W. A. Goddard, P. M. Henry, *Organometallics* **2009**, *28*, 1618.
[19] D. J. Nelson, R. Li, C. Brammer, *J. Am. Chem. Soc.* **2001**, *123*, 1564.
[20] a) J. A. Keith, J. Oxgaard, W. A. Goddard, *J. Am. Chem. Soc.* **2006**, *128*, 3132; b) J. A. Keith, R. J. Nielsen, J. Oxgaard, W. A. Goddard, *J. Am. Chem. Soc.* **2007**, *129*, 12342.
[21] a) C. J. Cramer, D. G. Truhlar, *Chem. Rev.* **1999**, *99*, 2161; b) C. J. Cramer, D. G. Truhlar, *Acc. Chem. Res.* **2008**, *41*, 760.
[22] J. Tomasi, B. Mennucci, R. Cammi, *Chem. Rev.* **2005**, *105*, 2999.
[23] A. Lledós, J. Bertrán, *Tetrahedron Lett.* **1981**, *22*, 775.
[24] C. Bergquist, B. M. Bridgewater, C. J. Harlan, J. R. Norton, R. A. Friesner, G. Parkin, *J. Am. Chem. Soc.* **2000**, *122*, 10581.
[25] C. A. Sandoval, T. Ohkuma, K. Muñiz, R. Noyori, *J. Am. Chem. Soc.* **2003**, *125*, 13490.
[26] C. P. Casey, J. B. Johnson, S. W. Singer, Q. Cui, *J. Am. Chem. Soc.* **2005**, *127*, 3100.
[27] C. Hedberg, K. Källström, P. I. Arvidsson, P. Brandt, P. G. Andersson, *J. Am. Chem. Soc.* **2005**, *127*, 15083.
[28] a) G. Kovács, G. Schubert, F. Joó, I. Pápai, *Organometallics* **2005**, *24*, 3059; b) G. Kovács, G. Schubert, F. Joó; I. Pápai, *Catal. Today* **2006**, *115*, 53.
[29] a) G. Kovács, G. Ujaque, A. Lledós, F. Joó, *Organometallics* **2006**, *25*, 862; b) A. Rossin, G. Kovács, G. Ujaque, A. Lledós, F. Joó, *Organometallics* **2006**, *25*, 5010.
[30] A. Comas-Vives, C. González-Arellano, A. Corma, M. Iglesias, F. Sánchez, G. Ujaque, *J. Am. Chem. Soc.* **2006**, *128*, 4756.
[31] A. Comas-Vives, C. González-Arellano, M. Boronat, A. Corma, M. Iglesias, F. Sánchez, G. Ujaque, *J. Catal.* **2008**, *254*, 226.
[32] J. E. Jee, A. Comas-Vives, C. Dinoi, G. Ujaque, R. Van Eldik, A. Lledós, R. Poli, *Inorg. Chem.* **2007**, *46*, 4103.
[33] F. De Angelis, S. Fantacci, A. Sgamellotti, *Coord. Chem. Rev.* **2006**, *250*, 1497, and references therein.
[34] B. Ensing, F. Buda, M. C. M. Gribnau, E. J. Baerends, *J. Am. Chem. Soc.* **2004**, *126*, 4355.
[35] J. W. Handgraaf, E. J. Meijer, *J. Am. Chem. Soc.* **2007**, *129*, 3099.
[36] a) M. Bühl, R. Diss, G. Wipff, *J. Am. Chem. Soc.* **2005**, *127*, 13506; b) M. Bühl, R. Diss, G. Wipff, *Inorg. Chem.* **2007**, *46*, 5196.
[37] Y. Tateyama, J. Blumberger, T. Ohno, M. Sprik, *J. Chem. Phys.* **2007**, *126*, 204506.
[38] S. Y. Yang, T. Ziegler, *Organometallics* **2006**, *25*, 887.
[39] T. Ziegler, J. Autschbach, *Chem. Rev.* **2005**, *105*, 2695.
[40] C. N. Rowley, T. K. Woo, *Organometallics* **2008**, *27*, 6405.
[41] C. N. Rowley, T. K. Woo, *J. Am. Chem. Soc.* **2008**, *130*, 7218.
[42] a) A. Laio, M. Parrinello, *Proc. Natl. Acad. Sci. USA* **2002**, *99*, 12562; b) M. Iannuzzi, A. Laio, M. Parrinello, *Phys. Rev. Lett.* **2003**, *90*, 238302.
[43] Selected application of metadynamics for chemical reactions: a) M. Boero, T. Ikeda, E. Ito, K. Teralura, *J. Am. Chem. Soc.* **2006**, *128*, 16798; b) N. N. Nair, E. Schreiner, D. Marx, *J. Am. Chem. Soc.* **2006**, *128*, 14148; c) A. Stirling, M. Iannuzzi, M. Parrinello, F. Molnar, V. Bernhart, G. A. Luinstra, *Organometallics* **2005**, *24*, 2533; d) A. Rodriguez-Fortea, L. Vilà-Nadal, J. Poblet, *Inorg. Chem.* **2008**, *47*, 7745.
[44] See the Supporting Information for more information about the free-energy calculations including the definition of CNs, the parameters used in the simulations, and the time evolution of the CVs during the simulations.
[45] R. Car, M. Parrinello, *Phys. Rev. Lett.* **1985**, *55*, 2471.
[46] A. D. Boese, N. Doltsinis, N. C. Handy, M. Sprik, *J. Chem. Phys.* **2000**, *112*, 1670.
[47] S. Izvekov, G. A. Voth, *J. Chem. Phys.* **2005**, *123*, 44505. For additional tests, see the Supporting Information.
[48] a) N. Troullier, J. L. Martins, *Phys. Rev. B* **1991**, *43*, 1993; b) See the Supporting Information for additional details of the test.
[49] CPMD v3.11. Copyright IBM Corp 1990–2007, Copyright MPI für Festkörperforschung Stuttgart 1997–2001.
[50] D. Marx, J. Hutter, *Ab initio Molecular Dynamics: Basic Theory and Advanced Methods*, Cambridge University Press, New York, **2009**.
[51] A. Laio, A. Rodriguez-Fortea, F. L. Gervasio, M. Ceccarelli, M. Parrinello, *J. Phys. Chem. B* **2005**, *109*, 6714.
[52] R. H. Crabtree *The Organometallic Chemistry of the Transition Metals*, Wiley, New York, **2005**.
[53] J. E. House, *Inorganic Chemistry*, Academic Press, New York, **2008**.
[54] L. I. Elding, Ö. Gröning, *Inorg. Chem.* **1978**, *17*, 1872.
[55] Within the CPMD calculation framework, the solvation of a proton is described properly because the explicit solvent molecules provide a realistic environment for solvation, and together with the ab initio methodology the most important many-body effects are included into the simulation, as opposed to the implicit solvation models. The methodology—without any a posteriori corrections—has already been successfully applied for various chemical processes that feature proton transfer, such as water autoionization (refs. [56], [57], and [58]) acetic-acid dissociation (ref. [59]), or various other proton-transfer processes (refs. [60] and [61]) These processes involve the protonation of a solvent H_2O molecule to form H_3O^+ species in its hydrated form. These studies demonstrate that the CPMD methodology is in fact very successful in describing the proton-transfer

mechanism not only in terms of structural and dynamical changes, but also in terms of activation barriers. More information can be found in a related useful review written by D. Marx (ref. [62]).
[56] P. L. Geissler, C. Dellago, D. Chandler, J. Hutter, M. Parrinello, *Science* **2001**, *291*, 2121.
[57] B. L. Trout, M. Parrinello, *Chem. Phys. Lett.* **1988**, *143-153*, 343.
[58] B. L. Trout, M. Parrinello, *J. Phys. Chem. A* **1999**, *103*, 7340.
[59] J. M. Park, A. Laio, M. Iannuzzi, M. Parrinello, *J. Am. Chem. Soc.* **2006**, *128*, 11318.
[60] K. Leung, S. B. Rempe, *J. Chem. Phys.* **2005**, *122*, 184506.
[61] M. De Vivo, B. Ensing, M. Dal Peraro, G. A. Gómez, D. W. Christianson, M. L. Klein, *J. Am. Chem. Soc.* **2007**, *129*, 387.
[62] D. Marx, *ChemPhysChem* **2006**, *7*, 1848; addendum: D. Marx, *ChemPhysChem* **2007**, *8*, 203.
[63] Z. Chval, M. Sip, J. V. Burda, *J. Comput. Chem.* **2008**, *29*, 2370.
[64] Static B3LYP calculations show that the *trans* complex is 8 kcal mol^{-1} more stable than the *cis*.
[65] J. J. Cruywagen, R. J. Kriek, *J. Coord. Chem.* **2007**, *60*, 439.
[66] A. H. Hoveyda, D. A. Evans, G. C. Fu, *Chem. Rev.* **1993**, *93*, 1307.

Received: December 22, 2009
Revised: May 3, 2010
Published online: June 22, 2010

